Thermal-physical properties of nanoparticle-seeded nitrate molten salts

Awad, Afrah; Navarro, Helena; Ding, Yulong; Wen, Dongsheng

DOI:
10.1016/j.renene.2017.12.026

Accepted Manuscript

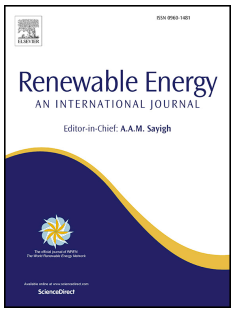

Thermal-physical properties of nanoparticle-seeded nitrate molten salts

Afrah Awad, Helena Navarro, Yulong Ding, Dongsheng Wen

PII: S0960-1481(17)31222-3

DOI: 10.1016/j.renene.2017.12.026

Reference: RENE 9523

To appear in: *Renewable Energy*

Received Date: 4 October 2017

Revised Date: 25 November 2017

Accepted Date: 4 December 2017

Please cite this article as: Awad A, Navarro H, Ding Y, Wen D, Thermal-physical properties of nanoparticle-seeded nitrate molten salts, *Renewable Energy* (2018), doi: 10.1016/j.renene.2017.12.026.

Thermal-physical properties of nanoparticle-seeded nitrate molten salts

Afrah Awad[1], Helena Navarro[2], Yulong Ding[2], Dongsheng Wen[3.1*]

[1]School of Chemical and Process Engineering, University of Leeds, UK

[2]School of Chemical Engineering, University of Birmingham, Birmingham, UK

[3]School of Aeronautic Science and Engineering, Beihang University, China

Email: d.wen@buaa.edu.cn & d.wen@leeds.ac.uk

Abstract

Molten salts have been used extensively as energy storing materials, however, their thermophysical properties, such as specific heat capacity and thermal conductivity have limited their applications. In this study, potassium nitrate and sodium–potassium nitrate ($NaNO_3$:KNO_3 with 60:40 molar ratio) are used as the base salts with different types of nanoparticles, which are iron oxide (Fe_2O_3), titanium dioxide (TiO_2) and copper oxide (CuO) over a wide range of temperatures up to 773 K. Laser flash analysis is used to measure thermal diffusivity and dynamic scanning calorimeter for specific heat (latent heat and melting temperature) of the molten salts and nanosalts. The addition of Fe_2O_3 into sodium–potassium nitrate salt increases thermal diffusivity up to 50%. Moreover, the highest increase in the latent heat reaches 14.45% at 1 wt. % CuO-binary nitrate salt. In addition, the total thermal energy storage of nanosalt increases up to 6% including both of sensible and latent heat. The formation of the interface layer between nanoparticles and salts could be the reason behind this enhancement in sensible and latent heats. The morphology of nanosalt measured by scanning electron microscopy showed a heterogeneous dispersion of nanoparticles, including agglomerated areas that could be sometimes responsible for the degradation of the performance.

Keywords: nanofluid, nitrate salt, specific heat capacity, latent heat, thermal energy storage, thermal diffusivity.

1. Introduction

Solar energy is a promising renewable energy source for our energy future, (Thirugnanasambandam et al., 2010), but can be only used during the daylight. An integration with a storage system must be done to ensure the reliability and availability of the system. Solar energy can be stored in three different forms as sensible heat, latent heat or in thermochemical form. Thermochemical reactions could provide higher energy storage density but it needs very complex systems to control these reactions.

Molten salt is generally used to store energy in sensible/latent forms. For example, most of the concentrated solar thermal power plants have been integrated with sensible storage tanks, i.e., one hot tank and one cold tank to store the energy up to 663 K. Considering that the melting temperature of solar salt ($NaNO_3$: KNO_3 with 60:40 molar ratios) is 505 K and for potassium nitrate (KNO_3) is around 607 K, any of them is a good choice for sensible heat storage (Chieruzzi et al., 2013, Chieruzzi et al., 2015). Another advantage of molten salt is its higher energy density due to its change phase with an approximately constant temperature giving a higher latent heat, e.g. the latent heat of KNO_3 is around 91.61 kJ/kg and solar salt is 110.01 kJ/kg (Chieruzzi et al., 2013, Chieruzzi et al., 2015a). The use of molten salt as a phase change material (PCM) for solar thermal applications has been investigated by many researchers such as (Feldhoff et al., 2012, Laing et al., 2009, Pfleger et al., 2015, Luo et al. 2017). However, their limited thermo-physical properties such as thermal conductivity, k, (in the range from 0.1-0.6 W/m. K (Kong et al., 2014)) and specific heat capacity (cp) have prevented its wide applications.

Nanoparticles have been recently proposed to solve the problem of low cp/k values of the nitrate molten salt. Many work have shown that dispersing nanoparticles to a base salt (here called nano-salt) at low concentrations could increase the cp value, but the results are inconclusive. There are different types of nitrate molten salt studied, including single nitrate salt, binary or ternary nitrate salt, which are briefly reviewed below. Chieruzzi et al. (2015b) studied the effect of silica, alumina and hybrid silica-alumina nanoparticles on single nitrate salt (KNO_3) salt. On the other hand, Lasfargues et al. (2015) studied the effect of dispersing CuO and TiO_2 nanoparticles on a binary nitrate (solar salt) and showed that the maximum increase

in cp was 10.48 % at 713 K for 0.1 wt. % CuO-solar salt. Moreover, different types of nanoparticles, with different concentrations and size have been dispersed into a binary nitrate solar salt to improve the cp of nanosalt (Andreu-Cabedo et al., 2014, Chieruzzi et al., 2013, Dudda and Shin, 2013, Lu and Huang, 2013, Riazi et al., 2016, Schuller et al., 2015, Luo et al., 2017). Others investigated the effect of dispersing silica, multi-walled carbon nanotubes, hybrid silica-alumina, Mica, gold and alumina nanoparticles into nitrate solar salt (Andreu-Cabedo et al., 2014, Chieruzzi et al., 2013, Dudda and Shin, 2013, Jung and Banerjee, 2011, Lu and Huang, 2013, Niu et al., 2014, Riazi et al., 2016, Schuller et al., 2015). Some of their results showed a higher increase in cp of nanosalt, which was dependent on the types, sizes, and concentrations of nanoparticles used. Others showed different results. This increase or decrease in the literature for the cp values of the nanosalt samples could be related to different sources of the materials used either molten salt (with different purities and suppliers) or the nanoparticles (different sources of the purchased companies or supplied by the researchers themselves). In addition, different preparation protocols and measurement conditions could also be the reasons. In order to explain the enhancement in cp of nanosalt samples, the literature indicated that interfaces were formed between the molten salt and nanoparticles (Riazi et al., 2016, Luo et al., 2017). Another explanation is the increment in the thermal resistance due to the effect of nanoparticles, which own higher surface areas. However, the simple mixing model, which relays on higher cp of nanoparticles itself in most of the cases, is not applicable to the nanosalt case as the cp of the nanoparticle is still less than cp of the molten salt.

Furthermore, extensive studies have been conducted on the enhancement of thermal conductivity by adding nanoparticles, and a term ‘nanofluid’ was coined (Buongiorno et al., 2009, Chol, 1995). However, common liquids or base fluids generally are used in energy systems such as water, mineral oils and polyalphaolefins lubricant (PAO). Very limited work has been conducted on molten salts. For instance, thermal conductivity (k) of binary nitrate salt with Al_2O_3 nanoparticles was measured using the laser flash analysis (LFA), which showed that adding nanoparticle decreased k in a temperature range between 338 K- 427 K (Schuller et al., 2012). Additionally, Myers et al. (2016) measured the thermal conductivity of the solid phase for three different types of nitrate molten salts (i.e.,

potassium nitrate, sodium nitrate, and the potassium–sodium nitrate eutectic (54 weight percent potassium nitrate) with copper oxide (CuO) nanoparticles. Their results showed an increment in thermal conductivity of the nanosalt, due to the formation of nanostructures between the nanoparticles and the molten salt. On the other hand, Shin (2011) studied the thermal conductivity when dispersing silica nanoparticles (1 wt.%) in carbonate salt of lithium: potassium carbonate salt (Li_2CO_3: K_2CO_3 with 62:38 by molar ratio) up to 573 K. The results showed an enhancement in k by 37%-47%, and it was believed that smaller size of nanoparticles increment the interfacial thermal resistances resulted in a k decrease. They also indicated that none of the two models, The Hamilton_Crosser and Maxwell_Garnett models could predict the enhancement correctly.

It shall be noted that both cp and k, or thermal diffusivities, values are needed to assess the performance of a molten salt, including the storage capacity and charging/discharging behaviour. However, none of the work reported so far have reported these properties in one study. From the k side, none of the previous studies shows the effect of different nanoparticles on thermal conductivity over a wide range of temperatures up to 773 K by taking into consideration of both solid phase and liquid phase.

In this work, we investigate experimentally the thermal-physical properties (k, cp) of nanosalts to reveal the performance of nanoparticles. Different concentrations (0.5 wt. %, 1 wt. % and 1.5 wt. %) of Fe_2O_3, CuO and TiO_2 on single salt (KNO_3) and binary solar salt are studied. The thermal conductivity is determined by a laser flash analysis device; the thermal diffusivity data, including both solid and liquid phases, are measured up to 773 K. The cp, melting temperature, and heat of fusion are measured by a dynamic scanning calorimeter (DSC) device. In addition, material characterization is also reported by the scanning microscopy (SEM) and the DLS of the nanoparticles size.

2. Experiments

2.1 Material

The base material used for this study is nitrate molten salt. Sodium nitrate ($NaNO_3$) was purchased from (FISHER, Loughborough, UK) with 98% purity and potassium

nitrate (KNO_3) from (SIGA-ALDRICH, Suffolk, UK) with 98% purity. The additive materials were copper oxide (CuO) nanoparticles (<50 nm particle size) purchased from Sigma-Aldrich Company, and iron oxide (Fe_2O_3) nanoparticles (20–40 nm particle size) purchased from (iolitec-USA company). The commercial titanium dioxide (TiO_2) nanoparticles purchased from nanostructured & amorphous materials Inc., with purity of 99.8% and an average diameter of 50 nm.

The samples were prepared by the two-step method. Briefly, the nanoparticles were firstly mixed with molten salt and distilled water (30 ml), followed by a sonication process to ensure a good dispersion of nanoparticles within the sample. Then evaporation of water from the sample was conducted on a hot plate at a temperature around 423 K until the water was fully evaporated from the samples.

2.2 Measurement

i) Differential scanning calorimetry (DSC)

Specific heat capacity tests were performed on a Mettler Toledo DSC (Differential scanning calorimetry, DSC1, Mettler Toledo, Leicester, UK) for single salt, binary salt, nanoparticles (Fe_2O_3, CuO, and TiO_2) and nanosalt (with different concentrations of nanoparticles, e.g. 0.5 wt. %, 1 wt. % and 1.5 wt. %), as well as the latent heat, and $T_{melting}$ of molten salt and nanosalt. The sample was placed in the crucible made of platinum, sample‘s weight was in the range of 30 mg to 35 mg excluding the weight of the crucible in order to have enough materials to fill the pan but not too much to cause the overflow issue during the measurements. The sample was measured by an Ultra-microbalance Mettler Toledo balance (UMX2 Ultra-microbalance, Mettler Toledo, Leicester, UK) with an uncertainty of 0.1 µg. Sapphire was used as a standard material with known specific heat capacity values in the range of temperatures of the experiments. The heating method used was modelled at a rate of 423 K for 10 min, ramped from 423 K to 723 K at a rate of 10 K/min, then maintained isothermally for 10 min at 723 K and finally cooled down from 723 K to 423 K at -40 K/min. It shall be noted that the maximum temperature in case of KNO_3 base material is less than 673 K. The standard error of the DSC device used for this experiments is less than 2.29% and each sample tested for three times and they

show a repeatable and coincide results. The uncertainty of DSC measurements of different samples is shown in Tables (11-12).

ii) Laser flash analysis (LFA)

Laser flash analysis (laser flash analysis LFA, model LFA 427, Netzsch Company, Selb, Germany) device was implemented to measure thermal diffusivity of the sample. In the LFA measurement, the diffusivity was determined by heating the front face of the sample by a laser with simultaneous record of the temperature profile on the rear face

Three layers model is used in a LFA measurement. The sample is the layer with unknown diffusivity and the other two layers represent the samples' holder and the crucible lid with known properties, as shown in Figure (1). The elegance of the method lies in the fact that the troublesome measurement of the absolute quantity of laser energy absorbed by the sample and of the resulting absolute temperature increase is replaced with a more accurate and direct measurement of time and relative temperature increase.

In order to calculate the thermal conductivity of the samples, the values of density and the specific heat capacity are needed, and k can be calculated as shown in the Equation (1).

$$k = cp \times \rho \times a \qquad (1)$$

where k is thermal conductivity W/(m. K), cp is specific heat capacity J/(g. K) (measured in the DSC device), ρ is density in g/m^3 and a, is thermal diffusivity m^2/s. According to Janz et al. (1972), the density of binary nitrate solar salt can be calculated as a function of temperature depending on the Equation (2).

$$\rho = 2064.31 - (4.76248 \times 10^{-4} \times T^2) - (3.36495 \times 10^{-7} \times T^2) \qquad (2)$$

The range of temperatures in Equation (2) is from ambient temperature (298 K) up to 773 K.

For nanosalt Equation (3) has been used by (Vajjha et al., 2009):

$$\rho_{nanosalt} = (\varphi_{np} \times \rho_{np}) + ((1-\varphi_{np}) \times \rho_{salt}) \qquad (3)$$

where φ_{np} is concentration of nanoparticles, $\rho_{nanosalt,}$ ρ_{np} and ρ_{salt} are the density of nanosalt, nanoparticles and solar salt, respectively. Additionally, the density of solar salt is calculated from Equation (2) in the range of temperature from ambient temperature (298 K) up to 773 K. The density of nanoparticles is assumed as a constant value taken from the MSDS of the material. For instance, density of CuO nanoparticles equals 6320 kg/m^3 and density of Fe_2O_3 nanoparticles as 5240 kg/m^3. Therefore the density of nanosalt in Equation (3) is dependent on the same range of temperatures in Equation (2). Additionally, the uncertainty of LFA diffusivity measurements and calculated thermal conductivities of different samples are considered. Each sample is investigated three times, a repeatable results are found with a standard error less than 2.6% of thermal diffusivity measurements using the LFA instrument. Additionally, Figure (17) below shows the plot of thermal conductivity k vs temperatures, with the error bars of all the experiments data for different materials (solar salt and nanosalt). Moreover, Tables (13-14) illustrated the error of different tests for thermal diffusivity and thermal conductivity, respectively. The errors of thermal conductivity are the accumulated errors from the cp and thermal diffusivity measurements therefore they are higher than others (errors of cp and thermal diffusivity). However, the error are within acceptable values with the maximum value of 0.0496.

iii) Scanning electron microscopy

Morphology of the samples is performed by a scanning electron microscopy (scanning electron microscopy, SEM, model Hitachi SU8230, Hitachi company, Berkshire, UK) device. SEM was used to show the surface morphology of molten salt without and with nanoparticles. The samples were in powder form and their morphology before and after repeatable thermal cycles were studied.

iv) Dynamic light scattering

Dynamic light scattering DLS (dynamic light scattering DLS, Malvern Zetasizer ZS, Malvern Zetasizer, Malvern, UK) was used to measure the size of nanoparticles in this work. Nanoparticles were dispersed in distilled water and then measured in DLS where the intensity vs particles size was obtained. Three different samples of three

different nanoparticles (Fe_2O_3, CuO, and TiO_2) used in this work mixed with distilled water and sonicate before testing in the DLS device. We did not used any type of surfactant to stabilise the nanofluid, and as nanoparticles might have suffered from agglomeration, leading to a large particle size, shown in Figure (12). The maximum error analysis obtained was 3.4%.

3. Results and discussions

3.1 Specific heat capacity (cp)

The cp results showed that adding nanoparticles to any of the nitrate molten salt used in the experiments (either single salt (KNO_3) or binary salt (60 $NaNO_3$:40 KNO_3)) had either a positive or negative effect, depending on many factors such as concentration, size or type of the nanoparticles used.

Figures (2-3) indicate that nanoparticles significantly affect the specific heat capacity of nanosalt. For solid phase results, 1.5 wt. % samples have larger increments in cp of nano-binary salt. In a similar study by using silica nanoparticles, Chieruzzi et al. (2013) who reported that 1 wt. % silica-nanosalt had higher cp value than 0.5 wt. % or 1.5 wt.%. The slight difference might be due to the fact that different types of nanoparticles could behave differently with solar salt as well the differences in the preparation procedure between ours and the work of Chieruzzi et al. (2013). Chieruzzi et al. (2013) used an ultrasonic bath for 100 minutes and evaporated the water at 473 K, while in ours, a probe sonicator was used with 423 K to evaporate the water. The results of single salt, KNO_3, are highly depending on the type of nanoparticles used, which is similar to what concluded by Chieruzzi et al. (2015a).

Figure (3) shows the dispersion of nanoparticles in KNO_3 or binary salt increases the specific heat capacity of nanosalt at high temperature. However, this increase depends on the type of the base material, concentrations and type of nanoparticles. Mostly, TiO_2-nanosalt shows a decrease in the cp of nano-binary salt, as shown in Table (3). In contrast, Lasfargues et al. (2015) indicated a positive effect of TiO_2-nanosalt and CuO-nanosalt. This difference could be due to different preparation methods. For single salt case, Table (4) demonstrates that in most cases, cp increases with the concentrations of nanoparticles. According to Chieruzzi et al.

(2015a), 1 wt.% of silica-KNO_3 salt has higher cp than KNO_3 while 1 wt.% of alumina-KNO_3 salt has lower cp than KNO_3. This is in similar to the results we got for 1 wt. % nano-KNO_3 however, Chieruzzi et al. (2015a) did not study the effect of another concentration (0.5 wt.%). The increment of cp of nanosalt in solid phase is slightly higher than that of liquid phase especially for the case of solar salt as the base material, which is in agreement to Chieruzzi et al. (2017).

From Tables (1-4), Fe_2O_3 nanoparticles seem to be a good option to increase the cp of the solid/liquid phase of the base material (either binary solar salt or single KNO_3 salt) followed by CuO nanoparticles. TiO_2 nanoparticle gives a very small enhancement in cp of nanosalt or in most of the cases it decreases the cp value.

There are some models used to predict the improvement in the cp when nanoparticles are added and these models are mentioned by many researchers for example Seo and Shin (2014). The classical model of the effective specific heat can be given by Equation (4)

$$cp_{,nf} = \frac{\rho_{np}\, \emptyset v_{np}\, cp_{,np} + \rho_{salt}\, \emptyset v_{salt}\, cp_{,salt}}{\rho_{np}\, \emptyset_{vnp} + \rho_{salt}\, \emptyset_{vsalt}} \qquad \textbf{(4)}$$

Where $cp_{,nf}$, $cp_{,np}$ and $cp_{,salt}$ represent cp of nanosalt, nanoparticle, and salt. $\emptyset v_{np}$ and $\emptyset vsalt$ are the volume fraction of nanoparticles and salt, respectively. ρ_{np} and ρ_{salt} are the density of nanoparticle and salt, respectively.

The range of temperatures in Equation (4) depends on the tested material (nitrate salt), as shown below

- In case of binary solar salt (and nano-solar salt)
  Solid phase (423 K < Temperature < Tonset)
  Liquid phase (523 K < Temperature < 723 K)
- In case of KNO_3 salt (nano-KNO_3)
  Solid phase (473 K < Temperature < Tonset)
  Liquid phase (623 < Temperature < 668 K)

However, this model would not show any enhancement in cp unlike the most of the experimental results. This discrepancy is due to the lower value of cp of nanoparticles comparing to the salt. For instance, cp of Fe_2O_3 nanoparticle is smaller than that of a molten salt. Even the fact that cp of nanoparticles is larger, e.g. cp of

Fe_2O_3 around (0.9 J/g. K), which is slightly higher than its bulk material (0.84 J/g. K) in the range of (423 K – 723 K) as indicated by Snow et al. (2010). For more emphasis, we measured the cp of all nanoparticles used for the current experiments. In this experiments, cp of Fe_2O_3 equals to (0.9 J/g. K), cp of CuO equals to (0.59 J/g. K) and cp of TiO_2 is (1.06 J/g. K). Furthermore, Zhou and Wang (2003) referred that cp of bulk CuO was (0.54 J/ g. K). While the cp of CuO nanoparticles measured in the current experiment equals to (0.59 J/ g. K) which is slightly higher than cp of its bulk material. However, cp values of Fe_2O_3 / CuO/ TiO_2 nanoparticles are still lower than that of a molten salt. This indicates that the increases in cp are not due to the nanoparticle effect. Therefore, the classical model cannot predict the enhancement in cp of nanosalt where the cp of molten salt is larger than that of the nanoparticles used in the respective work. Therefore, this model needs to expand and include the other factors such as the interfacial area formed at the surface of the nanoparticle and the molten salt or other forces between nanoparticles and so on.

Moreover, higher surface area owned by nanoparticles causes an increase in the thermal resistance between nanoparticles and the molecules of the molten salt, resulting in a rise in the interfacial interaction between them, which could increase the cp of a nanosalt. Additionally, during the preparation of the nanosalt sample and due to the sonication and evaporation stages, molten salt molecules could form a compressed layer on the surface of nanoparticles. These interfacial layers could have different properties to the base material alone. Furthermore, these layers could higher c_p, which may lead to increase the cp of nanosalt according to the Equation (5)

$$cp_{nf} = \frac{\rho_{np}\,\emptyset v_{np}\; cp_{np} + \rho_c\,\emptyset v_c\; cp_c + \rho_{salt}\,\emptyset v_{salt}\; cp_{salt}}{\rho_{np}\,\emptyset v_{np} + \rho_c\,\emptyset v_c + \rho_{salt}\,\emptyset v_{salt}} \qquad (5)$$

Where $cp_{,c}$, $\emptyset v_c$ and ρ_c represent cp, volume fraction, and density of compressed layer (interfacial layer), respectively. Equation (5) has a same temperature range as Equation (4).

In addition, the mass fraction of these layers depends on size and concentrations of nanoparticles. It is assumed that the cp of an interfacial layer has a significant effect on the overall cp of nanosalt when there is no agglomeration of nanoparticles. For instance, an assumed value of cp=6.2 J/ (g. K) (of the interfacial layer) would predict

the experimental well. Other possible reasons that could have the higher effect on the cp of the nanosalt are the sedimentation of nanoparticles, the Van der Waals force, and surface charge between the nanoparticles, as well the attractive force among the nanoparticles. These forces would help the agglomerations of these nanoparticles, which impact badly on their dispersion in the nanosalt samples. Therefore, there is a need to find a proper surfactant that could work efficiently at this high temperature condition, which could help to solve the dispersion and stability issue of nanoparticles in the nanosalt samples. Furthermore, cp vs temperature with the error bars of all the experiments data are plotted for different materials (solar salt and nanosalt or KNO_3 and nano-KNO_3) for both solid phase and liquid phase in Figures (13-16).

2.2 Latent heat

Latent heat is extensively affected by dispersing nanoparticles into the molten salt. Particularly, 1 wt. % of Fe_2O_3 and CuO in binary salt, 0.5 wt. % of Fe_2O_3 and CuO-single salt, increases the latent heat. The maximum improvement was found within CuO-binary salt up to 15% and Fe_2O_3-single salt up to 3%. This increment in latent heat of nanosalt will result with more energy stored per unit volume.

An interface is formed during the preparation of nanosalt sample. This interface is due to the rearrangement of nanoparticles in the nanosalt sample. Therefore, nanosalt needs higher heat to melt this interfacial layers, which maybe one of the reasons for increasing latent heat. Additionally, clusters of nanoparticles could lead to an increase in the latent heat as suggested by Chieruzzi et al. (2015a) and Lasfargues et al. (2015). More heat is needed to melt these agglomerations. However, this increasing or decreasing of latent heat of different nanosalts depends on the places of the presence of nanoparticles in the nanosalt sample. One example of the current experiments is the increases in latent heat due to the addition of 1 wt. % CuO nanoparticles into the binary salt. From SEM result Figure (5), it is clearly shown the agglomerations of 1 wt. % CuO-nanosalt and this sample have a higher value of latent heat as the clustering required more heat to melt, resulting in an increment in latent heat. Additionally, as shown in Figure (6) of the samples tested by SEM results, there is a presence of the agglomerations and clustering of the

nanoparticles in the nanosalt samples. These results are consistent with the observation from Chieruzzi et al. (2015a) and Lasfargues et al. (2015) for the enhancements of latent heat of nanosalt samples.

Likewise, the melting point of a nanosalt is highly affected by the addition of nanoparticles in samples. $T_{melting}$ is decreased with an addition of nanoparticles in all cases. In particular, the $T_{melting}$ of binary salt is decreased by 5 K in cases of all nanosalt samples, i.e $T_{melting}$ of binary salt is 503 K while $T_{melting}$ of all the nanosalt is between 498 K and 499 K. Furthermore, similar behaviour is observed in the case of KNO_3 base material with a decrement in $T_{melting}$ of KNO_3-nanosalt samples by 1 K. This is similar to the results from Gimenez-Gavarrell et al. (2015), Chieruzzi et al. (2013), Lasfargues et al. (2015) and Chieruzzi et al. (2015a). According to Lasfargues et al. (2015), $T_{melting}$ decrease in nanosalt relies on the method of heat transfer over nanosalt sample and the size of clustering of theses nanoparticles. Moreover, nanoparticles in the sample could work as nucleation agents, which bring the phase change earlier in comparison with the base salt, (Gimenez-Gavarrell et al., 2015). Although this decrement in melting temperature is low, it still considers an advantage because it means the phase change starts earlier. As a result, melting time will reduce which improves the heat transfer in the storage system with the support of enhanced conduction by nanoparticles.

Furthermore, the base material in case of binary salt does not reach the eutectic point as the melting temperature happened in a range of temperature not in a single point. Because of this, the mixture binary salt behaves as a non-pure mixture showing that it needs more heat to be melted or freezing completely. According to Kramer and Wilson (1980), the addition of 60% molar ratio of $NaNO_3$ would result in a melting temperature of the binary salt in a temperature range 494 K > $T_{melting}$ > 514 K. On the other hand, KNO_3 with a composition of 100% have one value for the $T_{melting}$ 608 K as it is a pure single material (Kramer and Wilson, 1980), Figure (7). However, KNO_3 material used in this experiment was 98% pure. From the DSC measurements, $T_{melting}$ of KNO_3 was in a range caused by its non-purity. The purity of the material has an impact that influence the behaviour of the salt and nanosalt properties.

3.3 Total thermal energy storage (TES)

TES is the total amount of energy of the storage system by considering both sensible and latent heats. TES of the nanosalt samples is different from the TES of molten salt alone. There is an increase or decrease in the TES as shown in Tables (5 and 6). From Table (5), 1 wt. % of Fe_2O_3-binary salt and 0.5 wt. % of CuO-binary salt represent the maximum increment in TES this is due to accumulated increment of energy. For instance, 1 wt.% of Fe_2O_3-binary salt own a higher increase in latent heat than other concentrations alongside with the advantages of sensible increment in both solid and liquid phases. Although, 1 wt.% of CuO-binary salt gave the maximum increases in latent heat, it owns less increment in the sensible heat in comparison to the 0.5 wt.%. Therefore, 0.5 wt. % of CuO-binary salt gave a higher TES than that of 1 wt. % of CuO-binary salt.

It seems to be 0.5 wt. % in single salt (KNO_3) shows higher increases with 5.26% for 0.5 wt. % Fe_2O_3- KNO_3 as shown in Table (6). TES represents by the summation of sensible heat (in the range of working temperatures of solid and liquid phases) and of latent heat as shown in the following equations

$$q_{storage} = q_{sensible} + q_{latent} \quad (6)$$

As $$q_{sensible} = q_{sensible\ in\ solid\ phase} + q_{sensible\ in\ liquid\ phase} \quad (7)$$

$$q_{storage} = [\int_{T_{ambient}}^{T_{melt}} cp * dT + \int_{T_{liquid}}^{T_{max.}} cp * dT] + q_{latent} \quad (8)$$

The range of temperatures in Equation (8) depend on the tested material (nitrate salt), as shown below

- In case of binary solar salt (and nano-solar salt)
  $T_{ambient}$ = 423 K, $T_{max.}$ = 723 K,
- In case of KNO_3 salt (nano-KNO_3)
  $T_{ambient}$ = 473 K, $T_{max.}$ = 668 K.

In order to increase the storage capacity of the molten salt, an improvement in the thermophysical properties of the molten salt is required. Therefore adding nanoparticles to the base material (molten salt) indicated an increase in the sensible/latent storage. Most of the cases, nanosalt will have a higher cp and higher

latent heat than the base material (molten salt) and this leading to a higher efficiency of the storage system, which indicated a higher level of the solar thermal power plant efficiency. According to Feldhoff et al. (2012), 9 hour is the storage time inside a two tank (hot and cold sensible tanks) in the solar thermal plant. The working temperature in the cold and hot tanks are 565 K and 659 K respectively. Dispersing nanoparticles into the base material will improve the cp of the base material. 14% is the efficiency of TES using molten salt alone, (Feldhoff et al., 2012), while with nanosalt as a storage medium this efficiency will increases. For instance, at T= 659 K, sensible heat of solar salt is 220.744 J/kg. However, this sensible heat (220.744 J/kg) can be increased when dispersing 1.5 wt. % of CuO in solar salt to 233.044 J/kg. As a result, the sensible heat of the nano-binary salt increased by 5.6% in comparison to solar salt only, which mean increasing the efficiency of the TES system. Furthermore, at T=659 K, the value of cp of nanosalt (KNO_3+ 1 wt. % Fe_2O_3) equals to (1.253 J/kg. K) while cp of molten salt (KNO_3) = 1.1615 J/kg. K. Therefore the sensible heat increased by 7.88% with the presence of nanoparticles. This indicates the big impact of nanoparticles on the efficiency of the storage system.

3.4 Thermal conductivity

On the other hand, thermal conductivity (k) of binary solar salt, Fe_2O_3-nanosalt, and CuO-nanosalt were tested. The current results demonstrate that nanoparticles have a significant effect on the thermal conductivity of nanosalts both at low and high temperatures. Increasing concentration of CuO, from 0.5 wt. % to 1.5 wt. %, has a negative effect on thermal conductivity of nanosalt. In contrast, Fe_2O_3 nanoparticles always increase k of nanosalt except for the case 1 wt. % Fe_2O_3-nanosalt. It is concluded that small concentrations of nanoparticles are preferred for increasing k of nanosalt samples.

The increase in temperature leads to an increase in Brownian motion of particles and this may lead to the enhancement observed in k. Additionally, these nanoparticles have higher k values in comparison with the base salt and therefore when the nanoparticle is mixed with base salt it would lead to a high k. However, this increment in k of nanosalt depends on the additive material properties, such as concentration and the type of nanoparticles. For instance, the sample prepared by

the mixing of base salt and the additive material (Fe_2O_3) seems to be more conductive material than CuO-nanosalt ones as shown in Figure (8). This show the effect of nanoparticles types on the nanosalt samples. Moreover, the higher surface area of nanoparticles could be one of the reasons that causes an increases in thermal conductivity for the nanosalt samples. In addition, Fe_2O_3 nanoparticles have less particle size means higher surface area than CuO nanoparticles and this could be one of the reasons behind the high improvements in Fe_2O_3-nanosalt than CuO-nanosalt samples (Yoo et al., 2007). According to Hwang et al. (2006), k of nanofluid is affected by the conductivity of both base and additive materials, which could be the same case for the current results as both nanoparticles used here have higher conductivity than a thermal conductivity of molten salt. The improvements in k of nanosalt are largely affected by particles loading, the temperature range of the test, nanoparticles size and stability of the sample. The results of thermal conductivity are listed in Table (7).

Additionally, both nanoparticles (CuO or Fe_2O_3) almost show that the lowest concentration (0.5 wt. %) give more increment in thermal conductivity than higher concentrations (1 wt. % or 1.5 wt. %). Although, 1.5 wt. % Fe_2O_3-nanosalt give better enhancement than 1 wt. % Fe_2O_3-nanosalt case. As shown in Table (7), there is a maximum increment of nanosalt (in 0.5 wt. %) over the range of concentrations tested. Figure (9) shows the effect of weight fraction of nanoparticles on thermal conductivity.

In general, k of nanofluids increases with increasing the concentration of nanoparticle (Mintsa et al., 2009). However, Figure (9) does show a certain discrepancy as the results for 0.5 wt. % nanosalt is slightly above others concentrations. According to (Saidur et al., 2011), conductivity increases with particles loading. This has some differences with current work due to the effect of the base material. Molten salt behaves differently than water, in addition, the effect of the surface charge of molten salt could play an important role on the result of k-Temp result. Furthermore, Assael et al. (2005) mentioned that increases concentrations from 0.1 to 6 mass % give a decreasing in k by 0.3% to 5% in respective. This is in matching with the results we got as an increment in particle loading give a lower k. Although we tested Fe_2O_3-nanosalt and CuO-nanosalt, which are different from the material tested by Assael et al. (2005), their material was carbon nanotube-water

based material. It indicates the big effect of the concentration on the improvement of k of nanosalt. More work needs to be considered in order to measure k of nanosalt over a wide range of concentrations to compare the effect of k with nanoparticles' loading in the nanosalt samples.

In order to calculate thermal conductivity theoretically, we would like to consider the Hamilton-Crosser model as shown in Table (9). According to Hamilton-Crosser model, the predicted value of k is not matching the measurement values. There are some reasons that could cause this difference. One of these reasons is the assumption of the sample in theoretical part compared to the actual behaviour of sample during the experiments, as the equation assumed the same size of nanoparticles are dispersed homogeneously along the sample, whereas in the experiment, it is very difficult to achieve due to the agglomeration and sedimentation effects of nanoparticles in the nanosalt sample. This could be due to the effects of different forces such as Van der Waals and gravity forces as both could lead to sedimentation or agglomerations of nanoparticles. Therefore, the calculated values cannot predict the enhancement in k unless consideration is given to all the affected factors.

Furthermore, the heat transfer will be improved in case of nanosalt due to the advantages of both cp, thermal conductivity. Due to the effect of natural convection during the phase change any increase in specific heat capacity or thermal conductivity will causes an increase in the heat transfer rate according to Equation (9). From heat transfer correlation equation, Nusselt number (Nu) is related to Rayleigh number (Ra) with some correlations constants, e.g. (Nu=C Ra^n) as C and n are constant depending on the case. In addition, any increases in the Nu will causes an increment in the heat transfer coefficient according to (h=Nu*k/L)) where h is heat transfer coefficient, L is the characteristic length and k is thermal conductivity. Therefore, any increases in Nu will give a higher heat transfer.

$$Ra = \frac{g\,\rho^2\,\beta\,\Delta T\,L_c}{\mu} * cp * k \qquad (9)$$

3.5 Comparison with other results

In order to check the accuracy of our results data and to see how much the data we got are reliable, a comparison was carried out with the literature data.

Specific heat capacity and latent heat of molten salt and nanosalt samples have been compared with other experiments literature data. The average value of cp of the KNO_3 salt in Chieruzzi et al. (2015b) was reported to be (1.118 J/g. K) and in the current work is (1.19 J/g. K) in the liquid phase. The average value of cp of the binary solar salt ($NaNO_3$:KNO_3 with 60:40 molar ratio) for the liquid phase equals to 1.315 J/g. K in the range 523 K -768 K (Jung and Banerjee, 2011) and cp has a value equals to 1.38 J/g. K in the range 523 K- 723 K by the work of (Xie et al., 2016). In the current work, cp of the binary solar salt for the liquid phase equals to 1.37 J/ (g. K) in the range 523 K -723 K.

In order to compare the latent heat values of the current study, first of all, KNO_3 salt has 91.61 J/g and T_{onset} is 608.7 K according to Chieruzzi et al. (2015b), in similarity, the current study KNO_3 salt has a value equals to 93.89 J/g with T_{onset} is 605.47 K. Secondly, in the current study, the latent heat of solar salt equals to 107.03 J/g with T_{onset} is 492.11 K likely to 110.01 J/g and T_{onset} is 492.88 K by (Chieruzzi et al., 2013). The standard error of the DSC device used for this work is less than 2.29% and each sample is tested for three times, which show a repeatable and consistent results. However, the small different in the results between the literature and the current work are more related to the precision of the device used and the thermal cycle of the test along with the samples used (each salt purchased from different sources in literature papers and the current work) and the types of crucible used in DSC device may cause this little differences.

Additionally, the thermal conductivity of nitrate salt has been reported by (Serrano-López et al., 2013). At a range of temperature 523 K- 673 K, the difference between current experiment values and the literature seems to be acceptable in term of different method used to the measurements as shown in Figure (11).

According to Serrano-López et al. (2013), none of the cited literature has mentioned laser-flash analysis as a measurement device for thermal conductivity of molten salts. The methods were used for the measurements are transient hot wire, coaxial cylinder, rough hard sphere, etc. In our experiment, laser-flash analysis have been used to measure thermal diffusivity of the samples and with the input of known

values of density (based on the literature) and cp (based on our experiments), the thermal conductivity has been calculated, which is approximately matching with the reported values.

4. Conclusion

The specific heat capacity, $T_{melting}$, latent heat and thermal conductivity of nitrate molten salt were studied using differential scanning calorimetry and laser-flash analysis, respectively. Different types of nanoparticles (0.5 wt. %, 1 wt. % and 1.5 wt. %) were dispersed in single salt (KNO_3) and binary salt ($NaNO_3$:KNO_3 with 60:40 molar ratio) to achieve good properties. Using Fe_2O_3 nanoparticles, we got a higher improvement of cp up to 11% and thermal conductivity up to 60%. In particular, the latent heat was increased up to 15% with 1 wt. % CuO-binary salt. The storage energy was improved up to 6% with Fe_2O_3 nanoparticles in comparison to solar salt only, which mean an increase of the efficiency of the TES system. Moreover, an increase in the sensible energy of nano-KNO_3 by 7.88% was observed.

In summary, the use of nanosalt to store thermal energy is a potentially promising technique due to the improved thermal conductivity and heat capacity values, which could not only increase the energy storage density but also accelerate the charging/discharging process.

Acknowledgments Afrah Awad would like to express her gratitude to the high committee of education development in Iraq (HCED) for the financial support.

References

ANDREU-CABEDO, P., MONDRAGON, R., HERNANDEZ, L., MARTINEZ-CUENCA, R., CABEDO, L. & JULIA, J. E. 2014. Increment of specific heat capacity of solar salt with SiO2 nanoparticles. *Nanoscale research letters,* 9**,** 582.

ASSAEL, M., METAXA, I., ARVANITIDIS, J., CHRISTOFILOS, D. & LIOUTAS, C. 2005. Thermal conductivity enhancement in aqueous suspensions of carbon

multi-walled and double-walled nanotubes in the presence of two different dispersants. *International Journal of Thermophysics,* 26**,** 647-664.

BUONGIORNO, J., VENERUS, D. C., PRABHAT, N., MCKRELL, T., TOWNSEND, J., CHRISTIANSON, R., TOLMACHEV, Y. V., KEBLINSKI, P., HU, L.-W. & ALVARADO, J. L. 2009. A benchmark study on the thermal conductivity of nanofluids. *Journal of Applied Physics,* 106**,** 094312.

CHIERUZZI, M., CERRITELLI, G. F., MILIOZZI, A. & KENNY, J. M. 2013. Effect of nanoparticles on heat capacity of nanofluids based on molten salts as PCM for thermal energy storage. *Nanoscale research letters,* 8**,** 448.

CHIERUZZI, M., CERRITELLI, G. F., MILIOZZI, A., KENNY, J. M. & TORRE, L. 2017. Heat capacity of nanofluids for solar energy storage produced by dispersing oxide nanoparticles in nitrate salt mixture directly at high temperature. *Solar Energy Materials and Solar Cells,* 167**,** 60-69.

CHIERUZZI, M., MILIOZZI, A., CRESCENZI, T., TORRE, L. & KENNY, J. M. 2015a. A new phase change material based on potassium nitrate with silica and alumina nanoparticles for thermal energy storage. *Nanoscale research letters,* 10**,** 273.

CHIERUZZI, M., MILIOZZI, A., CRESCENZI, T., TORRE, L. & KENNY, J. M. 2015b. A new phase change material based on potassium nitrate with silica and alumina nanoparticles for thermal energy storage. *Nanoscale research letters,* 10**,** 1.

CHOL, S. 1995. Enhancing thermal conductivity of fluids with nanoparticles. *ASME-Publications-Fed,* 231**,** 99-106.

DUDDA, B. & SHIN, D. 2013. Effect of nanoparticle dispersion on specific heat capacity of a binary nitrate salt eutectic for concentrated solar power applications. *International journal of thermal sciences,* 69**,** 37-42.

FELDHOFF, J. F., SCHMITZ, K., ECK, M., SCHNATBAUM-LAUMANN, L., LAING, D., ORTIZ-VIVES, F. & SCHULTE-FISCHEDICK, J. 2012. Comparative system analysis of direct steam generation and synthetic oil parabolic trough power plants with integrated thermal storage. *Solar Energy,* 86**,** 520-530.

GIMENEZ-GAVARRELL, P., ROMANIN, V. D. & FERERES, S. Latent Heat of Fusion and Melting Temperature of Molten Salt Based Carbon Nanotube Suspensions Used as Phase Change Materials. ASME 2015 9th International Conference on Energy Sustainability collocated with the ASME 2015 Power

597 Conference, the ASME 2015 13th International Conference on Fuel Cell
598 Science, Engineering and Technology, and the ASME 2015 Nuclear Forum,
599 2015. American Society of Mechanical Engineers, V001T10A005-
600 V001T10A005.
601 HWANG, Y., AHN, Y., SHIN, H., LEE, C., KIM, G., PARK, H. & LEE, J. 2006.
602 Investigation on characteristics of thermal conductivity enhancement of
603 nanofluids. *Current Applied Physics,* 6**,** 1068-1071.
604 JANZ, G., KREBS, U., SIEGENTHALER, H. & TOMKINS, R. 1972. Molten salts:
605 Volume 3 nitrates, nitrites, and mixtures: Electrical conductance, density,
606 viscosity, and surface tension data. *Journal of Physical and Chemical*
607 *Reference Data,* 1**,** 581-746.
608 JUNG, S. & BANERJEE, D. 2011. Enhancement of heat capacity of nitrate salts
609 using mica nanoparticles. *Dev Strateg Mater Comput Des II: Ceram Eng Sci*
610 *Proc,* 32**,** 127-137.
611 KONG, L. B., LI, T., HNG, H. H., BOEY, F., ZHANG, T. & LI, S. 2014. Waste Energy
612 Harvesting. *Springer, New York*.
613 KRAMER, C. M. & WILSON, C. J. 1980. The phase diagram of NaNO3—KNO3.
614 *Thermochimica Acta,* 42**,** 253-264.
615 LAING, D., BAUER, T., STEINMANN, W.-D. & LEHMANN, D. 2009. Advanced high
616 temperature latent heat storage system-design and test results. *Effstock*
617 *2009, Abstract Book and Proceedings*.
618 LASFARGUES, M., GENG, Q., CAO, H. & DING, Y. 2015. Mechanical dispersion of
619 nanoparticles and its effect on the specific heat capacity of impure binary
620 nitrate salt mixtures. *Nanomaterials,* 5**,** 1136-1146.
621 LU, M.-C. & HUANG, C.-H. 2013. Specific heat capacity of molten salt-based
622 alumina nanofluid. *Nanoscale research letters,* 8**,** 292.
623 LUO, Y., DU, X., AWAD, A. & WEN, D. 2017. Thermal energy storage enhancement
624 of a binary molten salt via in-situ produced nanoparticles. *International Journal*
625 *of Heat and Mass Transfer,* 104**,** 658-664.
626 MINTSA, H. A., ROY, G., NGUYEN, C. T. & DOUCET, D. 2009. New temperature
627 dependent thermal conductivity data for water-based nanofluids. *International*
628 *Journal of Thermal Sciences,* 48**,** 363-371.

MYERS, P. D., ALAM, T. E., KAMAL, R., GOSWAMI, D. & STEFANAKOS, E. 2016. Nitrate salts doped with CuO nanoparticles for thermal energy storage with improved heat transfer. *Applied Energy,* 165**,** 225-233.

NETZSCH 2017. PART A - Theoretical background, LFA 427, Operating Instructions, 09.93. 1-32.

NIU, D., LU, Y. & WU, D. 2014. Development of a novel thermal storage molten-salt filled with nanoparticles for concentration solar plants. *Bulgarian Chemical Communications,* 46.

PFLEGER, N., BAUER, T., MARTIN, C., ECK, M. & WÖRNER, A. 2015. Thermal energy storage–overview and specific insight into nitrate salts for sensible and latent heat storage. *Beilstein journal of nanotechnology,* 6**,** 1487.

RIAZI, H., MESGARI, S., AHMED, N. A. & TAYLOR, R. A. 2016. The effect of nanoparticle morphology on the specific heat of nanosalts. *International Journal of Heat and Mass Transfer,* 94**,** 254-261.

SAIDUR, R., LEONG, K. Y. & MOHAMMAD, H. A. 2011. A review on applications and challenges of nanofluids. *Renewable and Sustainable Energy Reviews,* 15**,** 1646-1668.

SCHULLER, M., LITTLE, F., MALIK, D., BETTS, M., SHAO, Q., LUO, J., ZHONG, W., SHANKAR, S. & PADMANABAN, A. 2012. Molten Salt-Carbon Nanotube Thermal Energy Storage for Concentrating Solar Power Systems Final Report. Texas Engineering Experiment Station.

SCHULLER, M., SHAO, Q. & LALK, T. 2015. Experimental investigation of the specific heat of a nitrate–alumina nanofluid for solar thermal energy storage systems. *International Journal of Thermal Sciences,* 91**,** 142-145.

SERRANO-LÓPEZ, R., FRADERA, J. & CUESTA-LÓPEZ, S. 2013. Molten salts database for energy applications. *Chemical Engineering and Processing: Process Intensification,* 73**,** 87-102.

SHIN, D. 2011. *Molten salt nanomaterials for thermal energy storage and concentrated solar power applications.* Texas A&M University.

SNOW, C. L., LEE, C. R., SHI, Q., BOERIO-GOATES, J. & WOODFIELD, B. F. 2010. Size-dependence of the heat capacity and thermodynamic properties of hematite (α-Fe 2 O 3). *The Journal of Chemical Thermodynamics,* 42**,** 1142-1151.

662 THIRUGNANASAMBANDAM, M., INIYAN, S. & GOIC, R. 2010. A review of solar
663 thermal technologies. *Renewable and sustainable energy reviews,* 14**,** 312-
664 322.
665 VAJJHA, R., DAS, D. & MAHAGAONKAR, B. 2009. Density measurement of
666 different nanofluids and their comparison with theory. *Petroleum Science and*
667 *Technology,* 27**,** 612-624.
668 XIE, Q., ZHU, Q. & LI, Y. 2016. Thermal Storage Properties of Molten Nitrate Salt-
669 Based Nanofluids with Graphene Nanoplatelets. *Nanoscale Research Letters,*
670 11**,** 1-7.
671 YOO, D.-H., HONG, K. & YANG, H.-S. 2007. Study of thermal conductivity of
672 nanofluids for the application of heat transfer fluids. *Thermochimica Acta,* 455**,**
673 66-69.

Figures

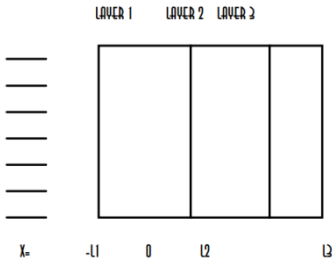

Figure 1 three layer model (NETZSCH, 2017)

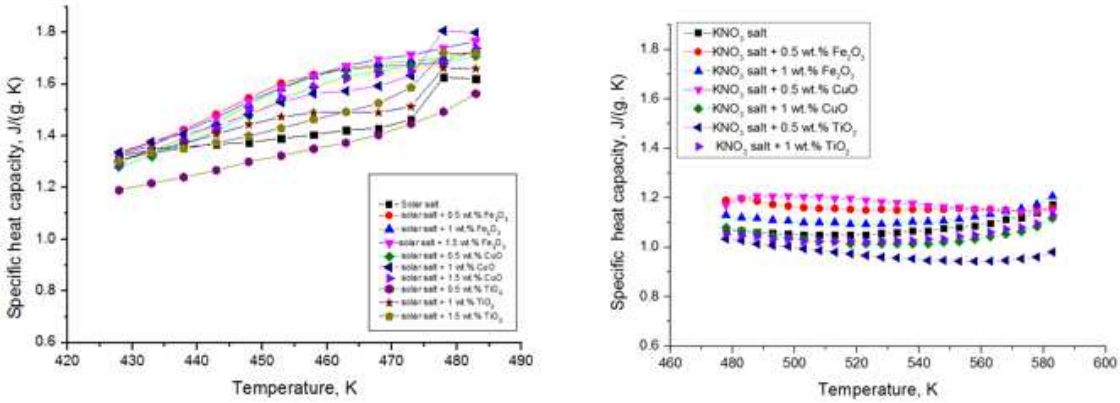

Figure 2 Solid phase of cp of different types and concentrations of nanoparticles dispersed into nitrate salt.

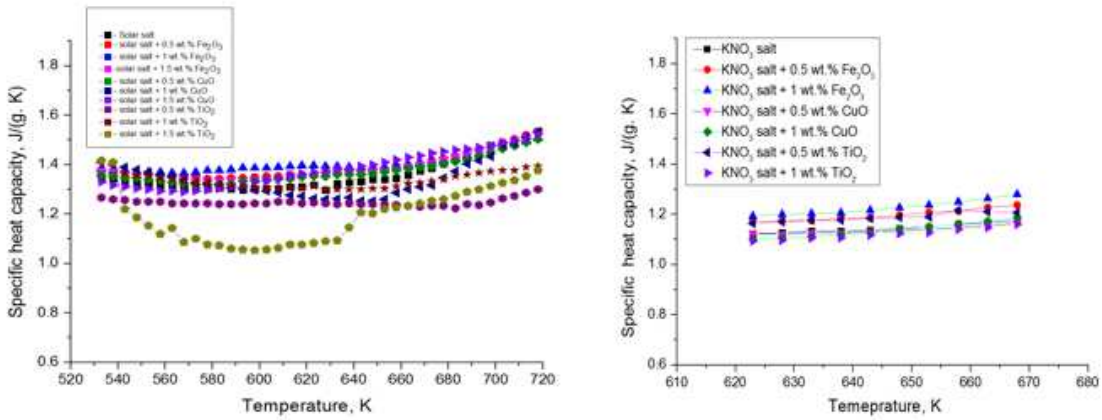

Figure 3 Specific heat capacity of liquid phase of different types and concentrations of nanoparticles dispersed in nitrate salt

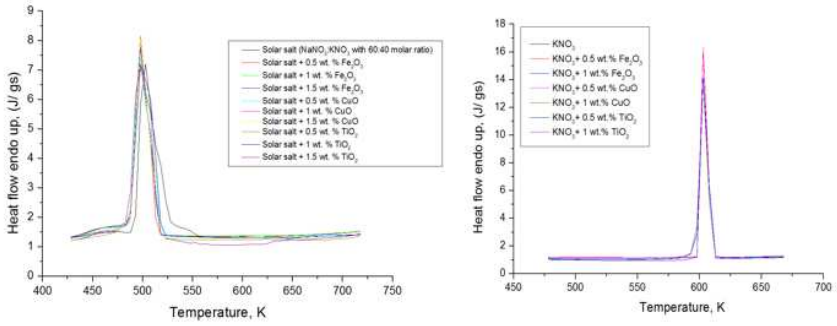

Heat flow vs temperature of binary salt and nanosalts

Heat flow vs temperature of KNO_3 and nano-KNO_3

Figure 4 Heat flow vs. temperature of salt and nanosalts

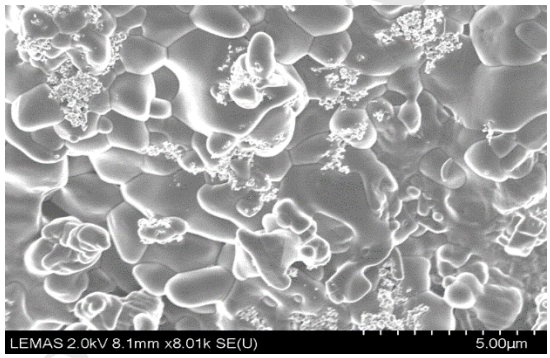

Figure 5 SEM test of 1 wt. % CuO dispersed in solar salt.

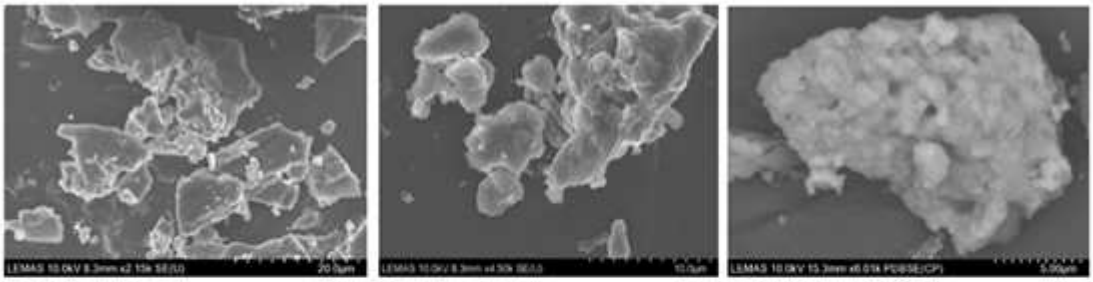

1 wt. % Fe_2O_3 dispersed in solar salt.

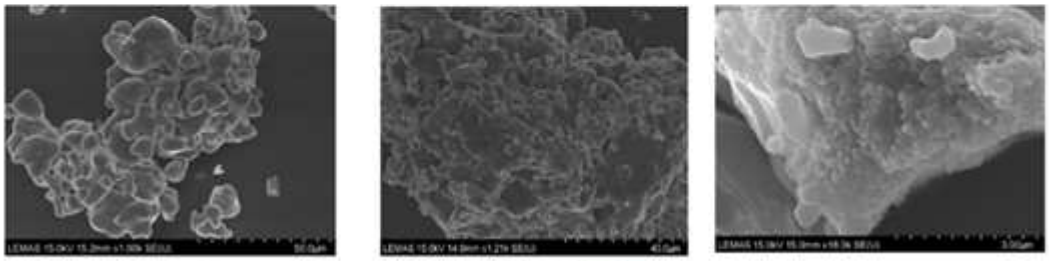

1 wt. % Fe_2O_3 dispersed in KNO_3 salt.

0.5 wt. % CuO dispersed in solar salt

0.5 wt. % CuO dispersed in KNO_3 salt.

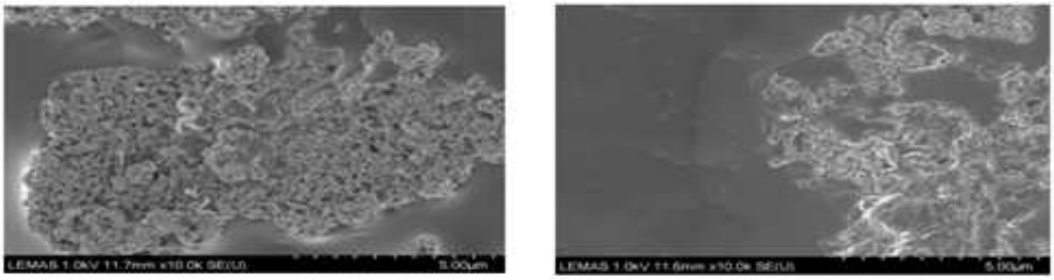

0.5 wt. % Fe_2O_3 dispersed in KNO_3 after melting/solidification cycles

0.5 wt. % TiO_2 dispersed in KNO_3 after melting/solidification cycles

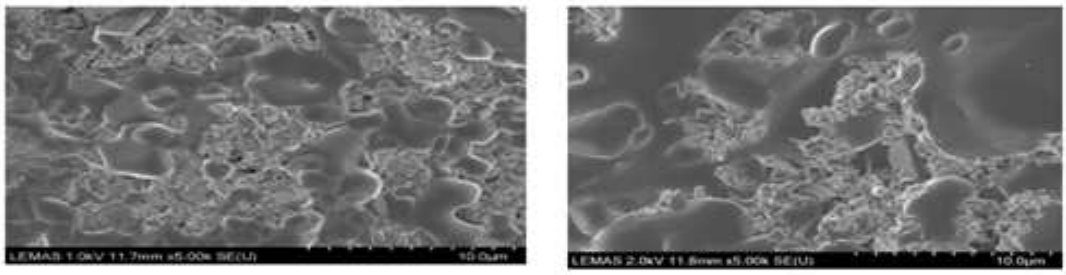

0.5 wt. % CuO dispersed in solar salt after melting/solidification

0.5 wt. % Fe_2O_3 dispersed in solar salt after melting/solidification

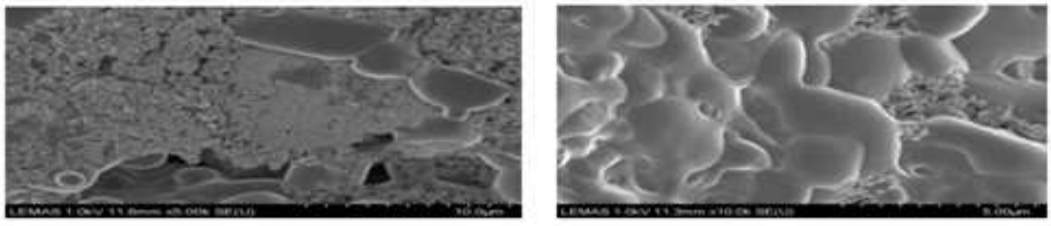

1 wt. % Fe_2O_3 dispersed in solar salt after melting/solidification

1 wt. % TiO_2 dispersed in solar salt after melting/solidification

Figure 6 SEM shows nanoparticle agglomerations after the preparation

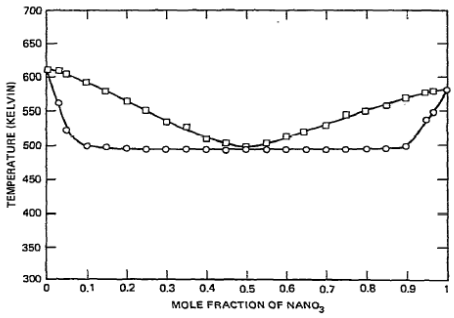

Figure 7 phase diagram of solar salt with different composition of $NaNO_3$ (Kramer and Wilson, 1980)

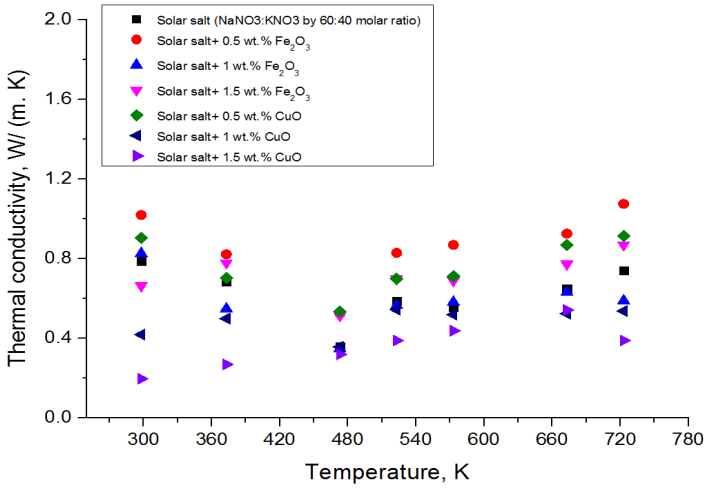

Figure 8 thermal conductivity vs. temperature of different samples.

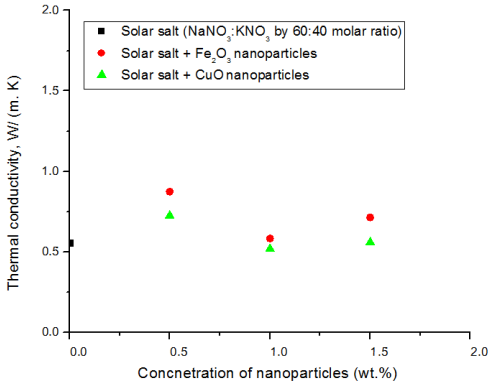

Figure 9 Thermal conductivity of nanosalt vs concentration of nanoparticles

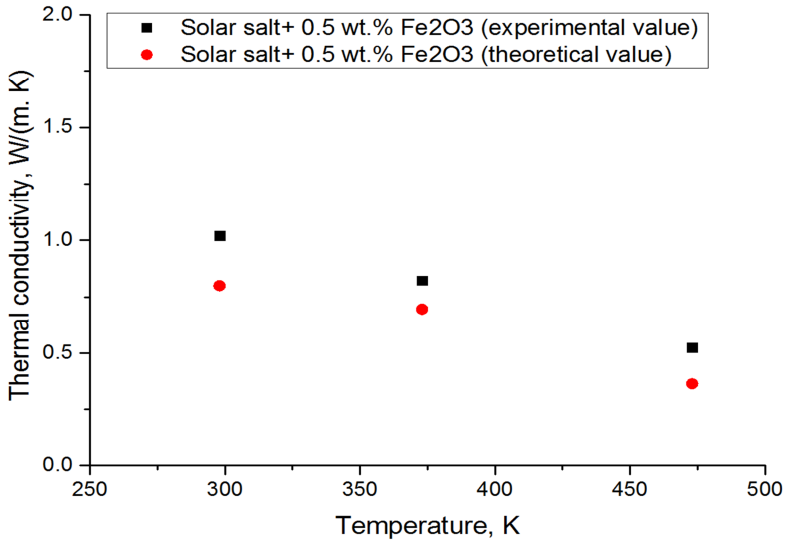

Figure 10 thermal conductivity vs temperature for 0.5 wt. % Fe_2O_3-nanosalt both experimental and calculated values

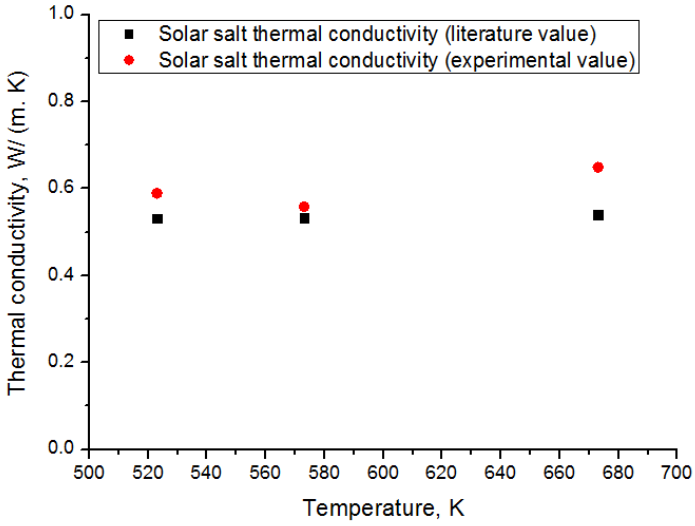

Figure 111 thermal conductivity of current experiment and in the literature (Serrano-López et al., 2013)

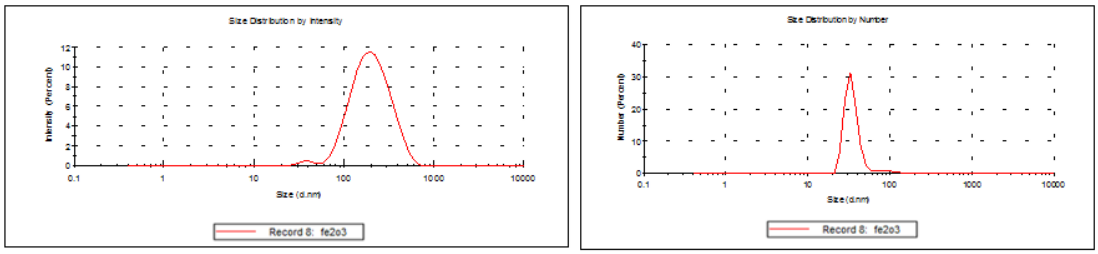

Fe_2O_3-nanofluid with average size of (175.5 nm)

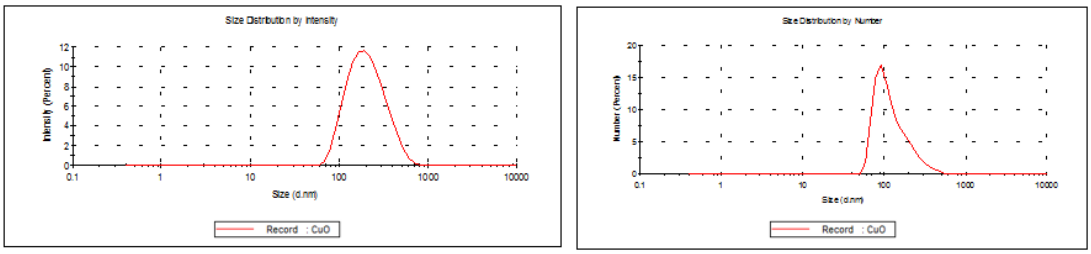

CuO-nanofluid with average size of (182.5 nm)

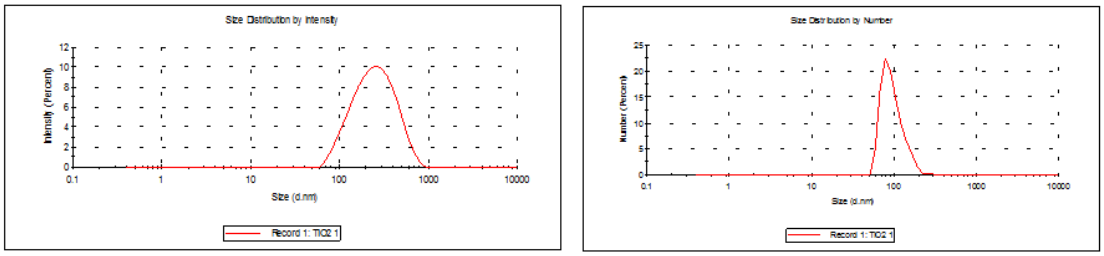

TiO2-nanofluid with average size of (214 nm)

Figure 122 Size measurement in DLS device for different nanofluid samples.

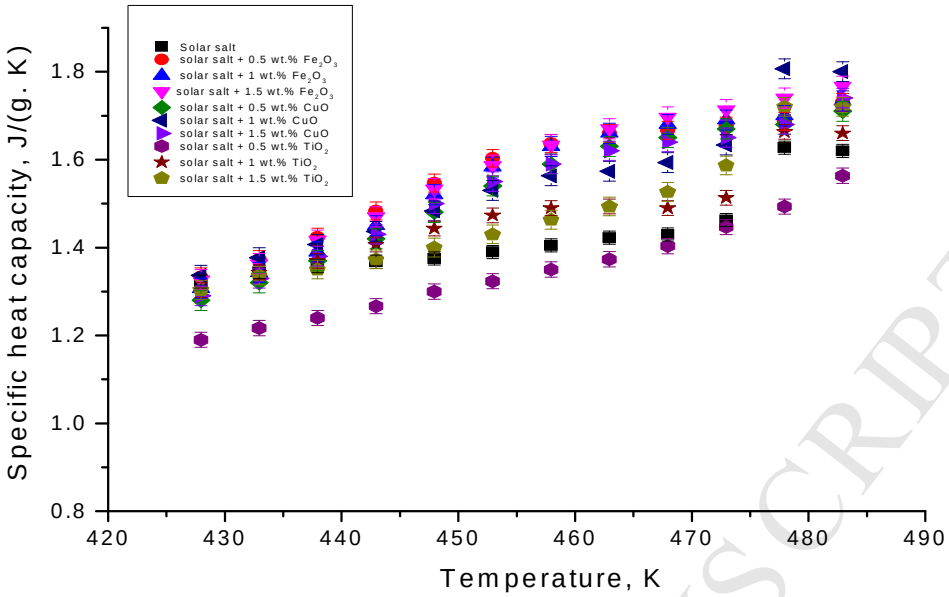

819

820 **Figure 13 Solid phase of cp of different types and concentrations of nanoparticles**
821 **dispersed into nitrate salt (binary solar salt) represented with error bars.**

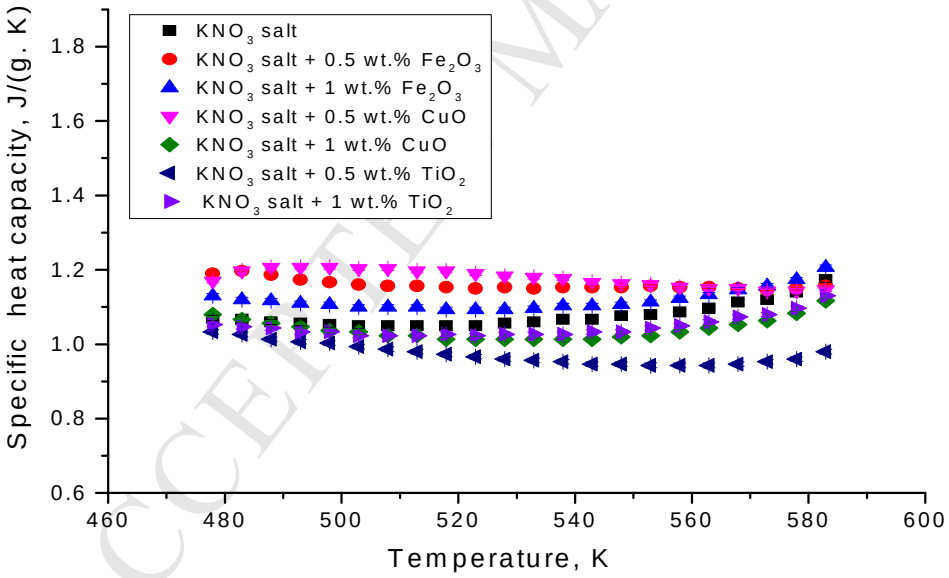

822

823 **Figure 14 Solid phase of cp of different types and concentrations of nanoparticles**
824 **dispersed into nitrate salt (KNO_3) represented with error bars.**

825

826

827

828

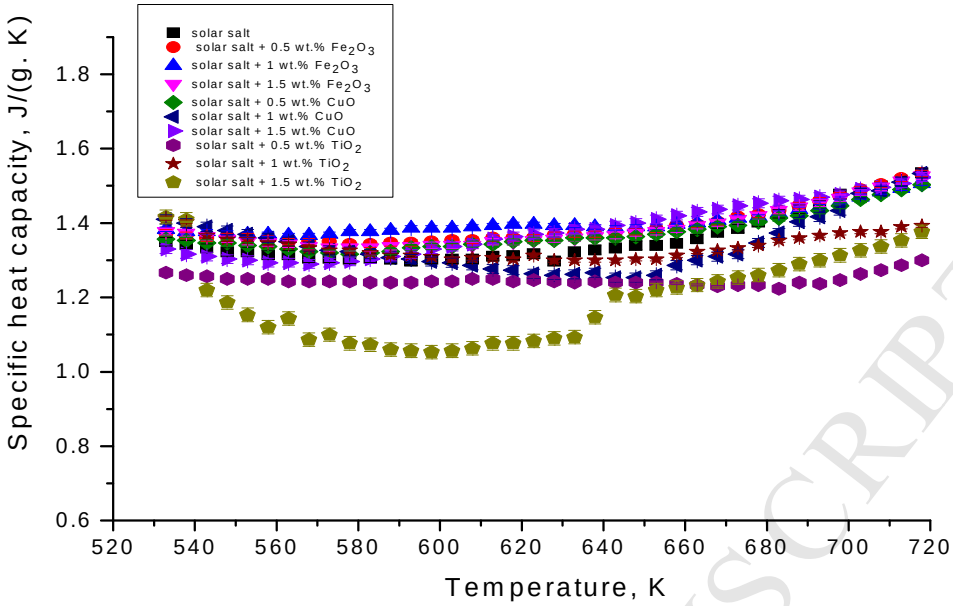

829
830 **Figure 15 liquid phase of cp of different types and concentrations of nanoparticles**
831 **dispersed into nitrate salt (binary solar salt) represented with error bars.**

832

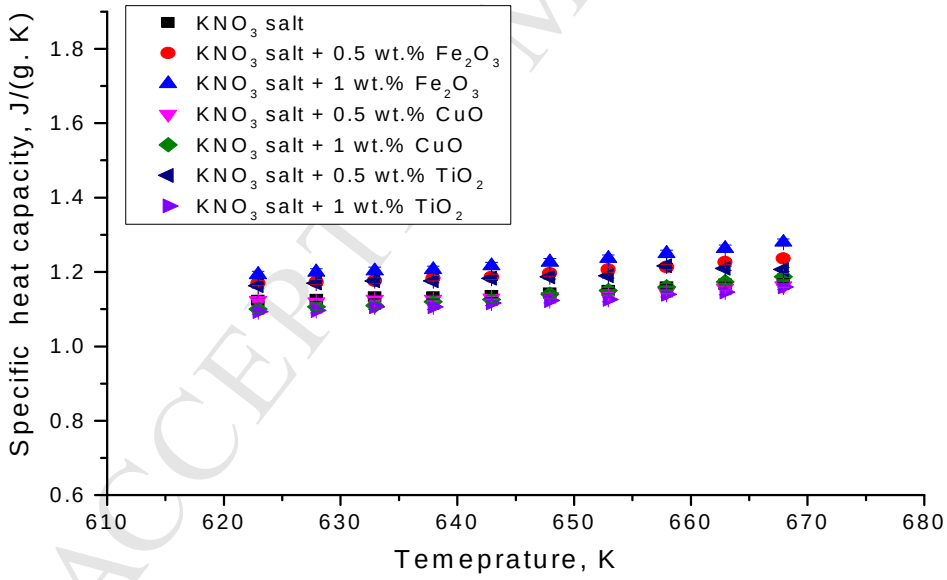

833
834 **Figure 16 liquid phase of cp of different types and concentrations of nanoparticles**
835 **dispersed into nitrate salt (KNO_3) represented with error bars.**

836

837

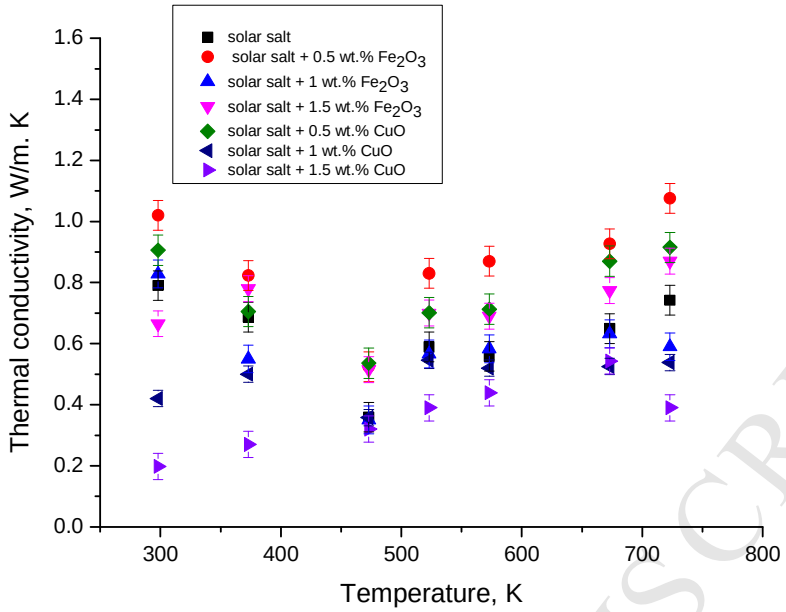

838

839 **Figure 17 Thermal conductivity with error bars of solar salt and nanosalt samples**

840

Tables

Table 1 Solid phase of cp (in range 423 K-488 K) of different types and concentrations of nanoparticles dispersed inside solar salt ($NaNO_3$:KNO_3 by 60:40 molar ratios).

Run	Solar salt	+ Fe_2O_3			+ CuO			+ TiO_2		
	-	0.5 wt.%	1 wt.%	1.5 wt.%	0.5 wt.%	1 wt.%	1.5 wt.%	0.5 wt.%	1 wt.%	1.5 wt.%
Run 1	1.43	1.67	1.63	1.67	1.59	1.37	1.64	1.27	1.31	1.3
Run 2	1.44	1.49	1.54	1.53	1.48	1.63	1.49	1.41	1.52	1.53
Run 3	1.43	1.54	1.51	1.53	1.51	1.56	1.48	1.36	1.53	1.52
Average	1.43	1.57	1.56	1.58	1.53	1.52	1.54	1.35	1.453	1.45
% Increase	-	9.8%	9.1 %	10.5%	7%	6.3%	7.7%	-5.6%	1.6%	1.4%

Table 2 Solid phase of cp (in range 473 K-588 K) of different types and concentrations of nanoparticles dispersed into KNO_3 salt.

Run	KNO3 salt	+ Fe_2O_3		+ CuO		+ TiO_2	
	-	0.5 wt.%	1 wt.%	0.5 wt.%	1 wt.%	0.5 wt.%	1 wt.%
Run 1	1.09	1.17	1.12	1.16	1.06	0.78	1.06
Run 2	1.072	1.15	1.11	1.151	1.03	1.085	1.04
Run 3	1.073	1.13	1.13	1.150	1.04	1.065	1.039
Average	1.078	1.15	1.12	1.154	1.043	0.98	1.046
% Increase	-	6.68%	3.9%	7.05%	-3.25%	-9.09%	-2.97%

Table 3 Liquid phase of cp (in range 523 K-723 K) of different types and concentrations of nanoparticles dispersed inside solar salt ($NaNO_3$:KNO_3 by 60:40 molar ratios).

Run	Solar salt	+ Fe_2O_3			+ CuO			+ TiO_2		
	-	0.5 wt.%	1 wt.%	1.5 wt.%	0.5 wt.%	1 wt.%	1.5 wt.%	0.5 wt.%	1 wt.%	1.5 wt.%
Run 1	1.38	1.36	1.33	1.37	1.36	1.37	1.35	1.14	1.27	0.9
Run 2	1.37	1.363	1.46	1.39	1.37	1.34	1.34	1.3	1.35	1.32
Run 3	1.35	1.46	1.42	1.39	1.4	1.32	1.45	1.31	1.39	1.30
Average	1.37	1.394	1.4	1.383	1.377	1.343	1.38	1.25	1.34	1.17
% Increase	-	1.75%	2.19%	0.95%	0.51%	-1.97%	0.73%	-8.76%	-2.19%	-14.6%

Table 4 Liquid phase of cp (in range 623 K-668 K) of different types and concentrations of nanoparticles dispersed into KNO_3 salt

Run	KNO3 salt	+ Fe_2O_3		+ CuO		+ TiO_2	
	-	0.5 wt.%	1 wt.%	0.5 wt.%	1 wt.%	0.5 wt.%	1 wt.%
Run 1	1.18	1.22	1.28	1.21	1.18	1.14	1.171

Run 2	1.2	1.28	1.27	1.18	1.22	1.28	1.17
Run 3	1.2	1.27	1.28	1.17	1.216	1.245	1.16
Average	1.19	1.26	1.28	1.187	1.205	1.222	1.167
% Increase	-	5.9%	7.56%	-0.25%	1.261%	2.69%	-1.93%

856

857

858 **Table 5 latent heat, onset temperature and total thermal energy storage capacity of**
859 **different types and concentrations of nanoparticles dispersed in solar salt**
860 **($NaNO_3$:KNO_3 by 60:40 molar ratios).**

Material	Latent heat (kJ/kg)	Onset temperature (K)	T_{onset} differences (K)	Total TES capacity (kJ/kg)	% TES
Pure salt	**107.03**	**492.11**	**-**	**466.83**	**-**
Salt + 0.5 wt. % Fe_2O_3	**109.27**	**489.22**	**2.89**	**482.27**	**3.31%**
Salt + 1 wt. % Fe_2O_3	**119.09**	**492**	**0.11**	**492.69**	**5.54%**
Salt + 1.5 wt % Fe_2O_3	**115.25**	**489.66**	**2.45**	**486.65**	**4.25%**
Salt + 0.5 wt % CuO	**118.08**	**489.01**	**3.1**	**485.28**	**3.95%**
Salt + 1 wt % CuO	**122.5**	**491.21**	**0.9**	**482.3**	**3.31%**
Salt + 1.5 wt % CuO	**110.32**	**490.05**	**2.06**	**478.72**	**2.55%**
Salt + 0.5 wt % TiO_2	**95.41**	**489.33**	**2.78**	**426.41**	**-8.66%**
Salt + 1 wt % TiO_2	**100.37**	**488.88**	**3.23**	**455.55**	**-2.42%**
Salt + 1.5 wt % TiO_2	**89.65**	**486.31**	**5.8**	**410.65**	**-12.03%**

861

862

863 **Table 6 latent heat, onset temperature and total thermal energy storage capacity of**
864 **different types and concentrations of nanoparticles dispersed inside KNO_3 salt.**

Material	Latent heat (kJ/kg)	Onset temperature (K)	T_{onset} differences (K)	Total TES capacity (kJ/kg)	% TES
KNO_3 salt	**93.89**	**605.47**	**0**	**331.47**	**-**
KNO_3 salt + 0.5 wt. % Fe_2O_3	**96.41**	**605.12**	**0.35**	**348.91**	**5.26%**
KNO_3 salt + 1 wt. % Fe_2O_3	**94.08**	**598.53**	**6.94**	**345.28**	**4.17%**
KNO_3 salt + 0.5 wt % CuO	**95.14**	**605.3**	**0.17**	**340.78**	**2.81%**
KNO_3 salt + 1 wt % CuO	**94.42**	**603.78**	**1.69**	**329.65**	**-0.55%**
KNO_3 salt+ 0.5 wt % TiO_2	**91.02**	**600.56**	**4.91**	**321.02**	**-3.15%**
KNO_3 salt+ 1 wt % TiO_2	**92.9**	**598.55**	**6.92**	**324.66**	**-2.05%**

865

Table 7 thermal conductivity (k, W/m. K) of different types and concentrations of nanosalt

T, K	Molten salt	Molten salt+ 0.5 wt.% Fe_2O_3	Molten salt+ 1 wt.% Fe_2O_3	Molten salt+ 1.5 wt.% Fe_2O_3	Molten salt+ 0.5 wt.% CuO	Molten salt+ 1 wt.% CuO	Molten salt+ 1.5 wt.% CuO
298	0.79	1.02	0.828	0.665	0.906	0.42	0.198
373	0.687	0.823	0.55	0.78	0.705	0.5	0.27
473	0.359	0.524	0.35	0.515	0.536	0.358	0.32
523	0.589	0.83	0.566	0.7	0.701	0.545	0.39
573	0.558	0.87	0.583	0.69	0.713	0.52	0.439
673	0.649	0.927	0.632	0.774	0.87	0.525	0.543
723	0.742	1.076	0.59	0.87	0.915	0.538	0.39

Table 8 Enhancement in thermal conductivity of different types and concentrations of nanosalt

T, K	Molten salt+ 0.5 wt.% Fe_2O_3	Molten salt+ 1 wt.% Fe_2O_3	Molten salt+ 1.5 wt.% Fe_2O_3	Molten salt+ 0.5 wt.% CuO	Molten salt+ 1 wt.% CuO	Molten salt+ 1.5 wt.% CuO
298	29.1	4.81	-15.8	14.68	-46.84	-74.94
373	19.8	-19.94	13.54	2.62	-27.22	-60.7
473	45.96	-2.51	43.45	49.3	-0.28	-10.86
523	40.92	-3.9	18.85	19.02	-7.47	-33.79
573	55.91	4.48	23.66	27.78	-6.81	-21.33
673	42.84	-2.62	19.26	34.05	-19.11	-16.33
723	45.01	-20.49	17.25	23.32	-27.49	-47.44

Table 9 theoretical calculations of thermal conductivity for different types and concentrations of nanosalt

T, K	Molten salt+ 0.5 wt.% Fe_2O_3	Molten salt+ 1 wt.% Fe_2O_3	Molten salt+ 1.5 wt.% Fe_2O_3	Molten salt+ 0.5 wt.% CuO	Molten salt+ 1 wt.% CuO	Molten salt+ 1.5 wt.% CuO
298	0.8	0.81	0.821	0.802	0.814	0.826
373	0.696	0.705	0.714	0.697	0.708	0.718
473	0.364	0.369	0.374	0.364	0.37	0.375

878 **Table 10 Nomenclature**

Symbol	Definition	Symbol	Definition
Fe_2O_3	Iron oxide nanoparticles	DSC	Differential scanning calorimetry
TiO_2	Titanium dioxide nanoparticles	mg	Milligram
CuO	Copper oxide nanoparticles	min	Minute
$NaNO_3$	Sodium nitrate salt	LFA	Laser flash analysis
KNO_3	Potassium nitrate salt	m^3	Cubic meter
K	Kelvin	ρ	Density, g/ m^3
KJ	Kilo Joule	a	Thermal diffusivity m^2/s
kg	kilogram	T	Temperature, K
cp	Specific heat capacity, (J/g. K)	φ_{np}	Nanoparticle concentration, wt.%
k	Thermal conductivity, W/(m. K)	ρ_{np}	Nanoparticles density, g/ m^3
PAO	polyalphaolefins lubricant.	ρ_{salt}	Salt density, g/ m^3
Al_2O_3	Alumina nanoparticles	ρ_c	Compressed layer density, g/ m^3
LFA	laser flash analysis	$\rho_{nanosalt}$	Nanosalt density, g/ m^3
wt. %	Weight percent concentration	cp_{np}	Specific heat capacity of nanoparticles, J/(g. K)
Li_2CO_3	lithium carbonate salt	cp_{salt}	Specific heat capacity of salt, J/(g. K)
K_2CO_3	potassium carbonate salt	cp_{nf}	Specific heat capacity of nanosalt, J/(g. K)
SEM	scanning electron microscopy	cp_c	Specific heat capacity of compressed layer, J/(g. K)
DLS	Dynamic light scattering	$\emptyset v_{salt}$	Volume fraction of salt
nm	Nanometre	$\emptyset v_{np}$	Volume fraction of nanoparticles
ml	Millilitre	$\emptyset v_c$	Volume fraction of compressed layer
$T_{melting}$	Melting temperature, K	TES	Total thermal energy storage
$\mathbf{q_{storage}}$	Storage energy, J/kg	$q_{sensible}$	Sensible energy, J/kg
$\mathbf{q_{latent}}$	Latent energy, J/kg	$q_{sensible\ in\ solid\ phase}$	Sensible energy of solid phase, J/kg
$\mathbf{T_{ambent}}$	Ambient temperature, K	$q_{sensible\ in\ liquid\ phase}$	Sensible energy of liquid phase, J/kg
$\mathbf{T_{melt}}$	Melting temperature, K	Nu	Nusselt number
$\mathbf{T_{liquid}}$	Liquid phase temperature, K	Ra	Rayleigh number
$\mathbf{T_{max.}}$	Maximum temperature, K	C	Constant
h	Heat transfer coefficient, $W/(m^2. K)$	n	Constant parameter
Lc	characteristic length, m	β	Expansion coefficient, K^{-1}
g	Gravity, m/sec^2	μ	Viscosity, Pa.s
$\mathbf{\Delta T}$	Temperature difference, K	T_{onset}	Onset temperature, K

879

880

881 **Table 11 of error from DSC device for the cp measurements of solar salt and nano-solar**
882 **salt**

	Solar salt	+0.5 wt.% Fe_2O_3	+1 wt.% Fe_2O_3	+1.5 wt.% Fe_2O_3	+0.5 wt.% CuO	+1 wt.% CuO	+1.5 wt.% CuO	+0.5 wt.% TiO_2	+1 wt.% TiO_2	+1.5 wt.% TiO_2
Solid phase	0.015	0.0202	0.0227	0.0229	0.0227	0.0228	0.0221	0.0173	0.0167	0.0212
Liquid phase	0.011	0.0086	0.0059	0.0089	0.0081	0.0122	0.0118	0.0024	0.0053	0.0181

883

884 **Table 12 of error from DSC device for the cp measurements of KNO_3 and nano-KNO_3**
885 **salt**

	KNO3	+0.5 wt.% Fe_2O_3	+1 wt.% Fe_2O_3	+0.5 wt.% CuO	+1 wt.% CuO	+0.5 wt.% TiO_2	+1 wt.% TiO_2
Solid phase	0.0007	0.0029	0.0062	0.0049	0.006	0.0061	0.0059
Liquid phase	0.0056	0.0073	0.0092	0.0046	0.0094	0.0057	0.007

886

887 **Table 13 of error from LFA device for the diffusivity measurements of solar salt and**
888 **nanosalts samples.**

Solar salt	+0.5 wt.% Fe_2O_3	+1 wt.% Fe_2O_3	+1.5 wt.% Fe_2O_3	+0.5 wt.% CuO	+1 wt.% CuO	+1.5 wt.% CuO
0.0223	0.0266	0.0181	0.0206	0.0217	0.0128	0.0145

889

890 **Table 14 of error for the calculated thermal conductivity of solar salt and nanosalts**
891 **samples.**

Solar salt	+0.5 wt.% Fe_2O_3	+1 wt.% Fe_2O_3	+1.5 wt.% Fe_2O_3	+0.5 wt.% CuO	+1 wt.% CuO	+1.5 wt.% CuO
0.0485	0.0486	0.0453	0.0423	0.0496	0.0266	0.0429

892